Volume 12
Number 9
7 March 2021
Pages 3081–3362

Chemical Science

rsc.li/chemical-science

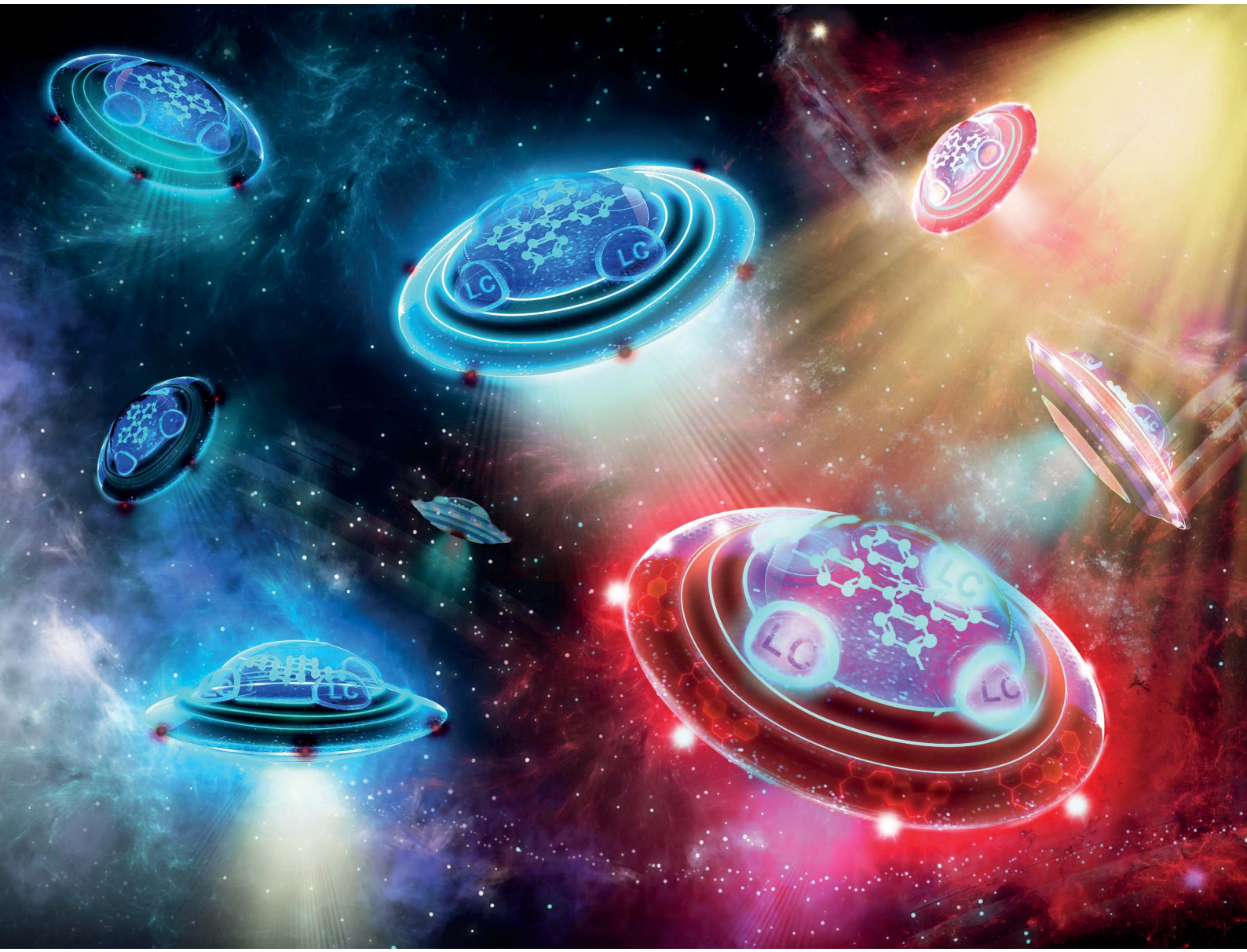

ISSN 2041-6539

ROYAL SOCIETY OF CHEMISTRY

EDGE ARTICLE

Zhen-Qiang Yu, Yue Wu, Alexander D. Q. Li *et al.*
Cooperatively assembled liquid crystals enable temperature-controlled Förster resonance energy transfer

Chemical Science

ROYAL SOCIETY OF CHEMISTRY

EDGE ARTICLE

View Article Online
View Journal | View Issue

Check for updates

Cite this: *Chem. Sci.*, 2021, **12**, 3146

All publication charges for this article have been paid for by the Royal Society of Chemistry

Cooperatively assembled liquid crystals enable temperature-controlled Förster resonance energy transfer†

Zhen-Qiang Yu, *[a] Xiaodong Li,[a] Wei Wan,[b] Xin-Shun Li,[a] Kuo Fu,[a] Yue Wu*[a] and Alexander D. Q. Li *[b]

Received 15th December 2020
Accepted 23rd January 2021

DOI: 10.1039/d0sc06838a

rsc.li/chemical-science

Balancing the rigidity of a π-conjugated structure for strong emission and the flexibility of liquid crystals for self-assembly is the key to realizing highly emissive liquid crystals (HELCs). Here we show that (1) integrating organization-induced emission into dual molecular cooperatively-assembled liquid crystals, (2) amplifying mesogens, and (3) elongating the spacer linking the emitter and the mesogen create advanced materials with desired thermal–optical properties. Impressively, assembling the fluorescent acceptor Nile red into its host donor designed according to the aforementioned strategies results in a temperature-controlled Förster resonance energy transfer (FRET) system. Indeed, FRET exhibits strong S-curve dependence as temperature sweeps through the liquid crystal phase transformation. Such thermochromic materials, suitable for dynamic thermo-optical sensing and modulation, are anticipated to unlock new and smart approaches for controlling and directing light in stimuli-responsive devices.

Open Access Article. Published on 26 January 2021. Downloaded on 6/18/2025 4:34:19 AM.
This article is licensed under a Creative Commons Attribution-NonCommercial 3.0 Unported Licence.

Introduction

The unique combination of photophysical and anisotropic fluid properties of highly emissive liquid crystals (HELCs) has attracted much attention recently.[1–9] Their potential applications have been widely studied in photonics and optoelectronics, such as field-effect transistors (FETs),[10,11] organic light emitting diodes (OLEDs),[12,13] organic light emitting transistors (OLETs),[14,15] and circularly polarized luminescence (CPL) materials.[16–18] Despite the promising prospects of HELCs, the synthetic challenges remain. Firstly, most luminogens suffer from aggregation caused quenching (ACQ), thus emitting weak or no emission in the condensed state. Additionally, liquid crystallinity can be hardly retained after introducing a π-conjugated fluorophore into linearly structured liquid crystals.[19–22] Therefore, resolving the conflicts between the rigid π-conjugated structure for strong emission and the flexible liquid crystals for assembly represents a dilemma and key scientific barrier in the further advancement of the field.

To solve this critical bottleneck, our strategy uses aggregation-induced emission (AIE) to incorporate an organization-induced luminogen (OIL)[23–29] into the liquid crystal to replace the ACQ-type luminogen[23] and covalently bonds such an AIE unit to mesogens to prevent segregation. By optimizing the mesogenic structures and spacer length between the AIE unit and mesogen, we fine tune the delicate balance of rigidity and flexibility in a "*step-by-step*" manner until a HELC is obtained (Fig. 1). By virtue of harnessing this strategy, an elaborate molecule consisting of an AIE group, 12-carbon linkers, and amplified mesogens, hereafter named TPE-12-4CB, is synthesized; it emits strongly in the condensed phase and has superb liquid crystallinity simultaneously.

Avoiding energy loss during emission and reabsorption, FRET transmits energy directly through space and plays a significant role in energy harvesting, such as collecting panchromatic light in a narrow waveband[30] or directing energy to specific reaction centers in the case of photosynthesis.[31] In consideration of the superb luminescence properties, a FRET-active luminescent solar concentrator (LSC)[32] has been fabricated. Using FRET, ratiometric temperature sensing has been achieved using semiconducting polymer dots.[33] Conversely, stimuli-responsive liquid crystals[34–36] without FRET also promise interesting interactions among light, mechanical force, and temperature.

Built upon the previous successes and our realization of HELCs, a thermochromic FRET system was constructed here by taking advantage of the temperature-controlled co-assembly of the luminescent donor TPE-12-4CB and acceptor Nile red to form liquid-crystal devices. Using stimuli-responsive optical materials to control and direct light represents a smart approach to solid-state devices because temperature can now be used to modulate light output. Sensing temperature-controlled FRET accurately and dynamically, a synchronous thermo-

[a]*College of Chemistry and Environmental Engineering, Shenzhen University, Shenzhen 518073, China. E-mail: zqyu@szu.edu.cn; wuyue@szu.edu.cn*

[b]*Department of Chemistry, Washington State University, Pullman, WA 99164, USA. E-mail: dequan@wsu.edu*

† Electronic supplementary information (ESI) available. See DOI: 10.1039/d0sc06838a

© 2021 The Author(s). Published by the Royal Society of Chemistry

Open Access Article. Published on 26 January 2021. Downloaded on 6/18/2025 4:34:19 AM.
This article is licensed under a Creative Commons Attribution-NonCommercial 3.0 Unported Licence.

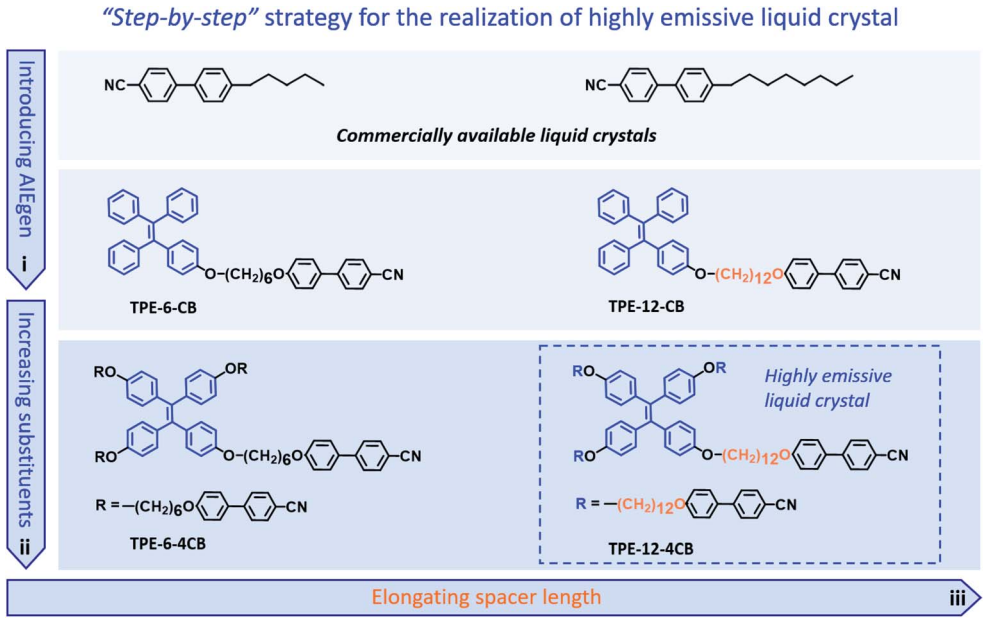

Fig. 1 Molecular engineering using AIE-genesis and a liquid crystal mesogen illustrates the *step-by-step* strategy for design and fabrication of a highly emissive liquid crystal. Step 1 introduces the AIE-core based on TPE for strong luminescence in condensed states; step 2 enhances emission efficiency by pushing π-electrons to the emissive core while amplifying mesogenic capability; step 3 elongates the mesogenic spacer for improving liquid crystallinity.

optical sensing (STOS) system was demonstrated, which simultaneously correlates sample temperature, FRET efficiency, and the fluorescence spectrum *in situ*.

Results and discussion

The cyanobiphenyl (CB) group is one of the most effective mesogens for liquid crystals because of its calamitic structure and molecular polarity; however, it is non-emissive under photoexcitation. Inspired by the molecular structure of 5-CB and 8-CB, we integrated an AIE-active tetraphenylethylene (TPE) unit with a CB group to obtain TPE-6-CB through the Williamson reaction with an excellent 90% yield (Fig. 1). TPE-6-CB shows intensive fluorescence at 450 nm under UV irradiation with a quantum yield (QY) of 4% (Fig. S1 in the ESI†). Similarly, TPE-12-CB also exhibits intensive fluorescence at 450 nm (Fig. S5 in the ESI†) with a QY of 6%. Compared to commercial LCs with low QY (5-CB: <1%), the introduction of an AIE unit is an effective strategy to endow LCs with the ability to emit luminescence, making it feasible for HELCs. After the luminescence properties were validated, the liquid crystallinity was investigated by differential scanning calorimetry (DSC) and polarized optical microscopy (POM). Interestingly, no typical liquid crystallinity was observed from the DSC curves of TPE-6-CB and TPE-12-CB during cooling (Fig. 2a), only one glass transition was observed at 39 °C and 19 °C, respectively, and no LC texture was captured by POM. It is concluded that the flexible assembly of LCs was suppressed by the rigid structure of TPE, indicating that one mesogenic CB was unable to induce the π-conjugated TPE to form an LC structure.

To realize HELCs, we next amplified the number of mesogenic substituents on TPE from one to four to obtain TPE-6-4CB (Fig. 1). Significantly, we found the fluorescence had an apparent enhancement with a 4.25-fold increase from 4% to 17% of the QY, demonstrating that the mesogenic substituent is capable of hindering the intramolecular rotation of TPE. Similarly, DSC and POM were employed to investigate the liquid crystallinity of TPE-6-4CB. Compared to TPE-6-CB, TPE-6-4CB has one crystallization peak at 133 °C during cooling (Fig. 2a) and no LC texture was captured by POM. These results demonstrate that the liquid crystallinity still could not be

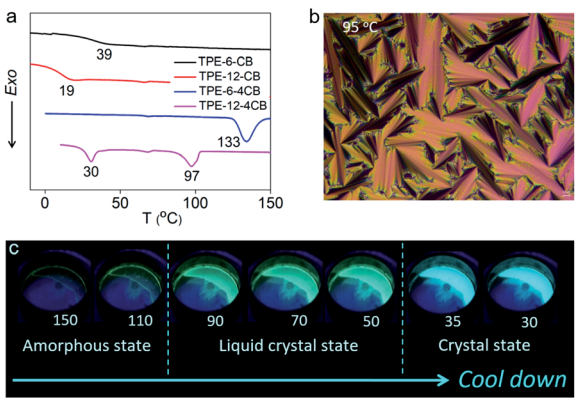

Fig. 2 (a) DSC traces of TPE-6-CB, TPE-12-CB, TPE-6-4CB, and TPE-12-4CB indicate disorder to order transitions, in particular, TPE-12-4CB changes from the amorphous phase to the liquid crystal phase (97 °C) and finally to the crystal phase (30 °C). (b) Image of the liquid crystal TPE-12-4CB hints at the typical fan-shaped texture of a smectic A phase, an ordered and layered structure. (c) Photographs of TPE-12-4CB reveal that luminescence intensifies as the material transitions from the disorder state to a reasonably ordered liquid crystal phase, and finally to a highly ordered solid crystal.

Open Access Article. Published on 26 January 2021. Downloaded on 6/18/2025 4:34:19 AM. This article is licensed under a Creative Commons Attribution-NonCommercial 3.0 Unported Licence.

realized *via* TPE-6-4CB. Again, the relatively short flexible spacer cannot decouple the interaction between TPE and amplified CB mesogens, and the twisted structure of TPE further frustrates the LC assembly, which requires flexibility.

Finally, to balance the rigidity of the emission core and flexibility of the liquid crystal assembly, we further elongated the spacer length between TPE and CB from six to twelve methylene units to obtain TPE-12-4CB (Fig. 1). This decoupling yields desired characteristics, and TPE-12-4CB exhibits two exothermic transitions at 97 and 30 °C in the DSC cooling process, which are assigned to isotropic liquid to LC and LC to crystal phase transitions, respectively. Typical fan-shaped focal conic textures were observed at 95 °C as shown in Fig. 2b indicating a smectic A (SmA) phase of the LC (Fig. S16 in the ESI†).[7] The wide-angle X-ray diffraction curve collected at 90 °C also identified the SmA phase (Fig. S17 in the ESI†). In this phase, mesogen CBs packed to form layered structures and TPE units stacked in the confined space to form a columnar structure. Taken together, these results precisely proved the liquid crystallinity of TPE-12-4CB.

To illustrate the luminescence behaviour of TPE-12-4CB in different states, thermochromic fluorescence images of TPE-12-4CB were recorded during the cooling cycle. In agreement with the DSC curve, two distinct luminescence behaviour-changes were found during the 130 → 30 °C cooling process (Fig. 2c). The first change occurred at ~90 °C, concomitant with the phase transition from isotropic liquid to the SmA phase of the LC, and the second change occurred at ~35 °C, accompanying the phase transition from the SmA phase of the LC to the solid crystal state. Furthermore, the QY of TPE-12-4CB increased to 27%, which was much higher than that of TPE-6-4CB. Thus, the "*step-by-step*" strategy solves the major dilemma to reconcile the rigid π-conjugated structure for strong emission and the flexible assembly for liquid crystallinity. This strategy creates a highly emissive TPE-12-4CB LC that has a wide LC temperature range (75–105 °C during heating and 30–97 °C during cooling).

Taking full advantage of exclusive HELC behaviour of TPE-12-4CB, we constructed a temperature-controlled luminescence modulator. Because Nile red absorbs from 400 to 600 nm, whose spectral range matches well with TPE-12-4CB emission (Fig. S18 in the ESI†), it was selected as an emission acceptor for the TPE-12-4CB donor for energy transfer. Doping Nile red (acceptor) into TPE-12-4CB (donor) without disrupting liquid crystal organization, a temperature-controlled FRET device has been constructed. As shown in Fig. 3a and c, Nile red emits strong orange fluorescence ($\lambda_{max} = 580$ nm) with high quantum efficiency (QY: 46%) in dilute solutions. However, it suffers from aggregation-caused quenching (ACQ), which limits its quantum yield (QY) to only 0.1%, a factor of 460-fold decrease, resulting in weak or even no emission in the condensed phases.

Inversely, TPE-12-4CB in dilute solution exhibits non-radiative decay or weak emission (QY: 0.3%) because of intramolecular rotation, but it becomes highly emissive in the condensed state ($\lambda_{max} = 472$ nm, QY: 27%), a 90-fold increase (Fig. 3b and d).[23] When AIE-active TPE-12-4CB and Nile red were assembled cooperatively to form an OIL, or organization-induced luminogen, the ACQ effect in the condensed state was remarkably eliminated (Fig. 3e) and the co-assembly exhibited temperature dependence of dual-colour emission. Tuning the Nile red to TPE-12-4CB ratio while exciting the system at 330 nm results in a dramatic strengthening of the Nile

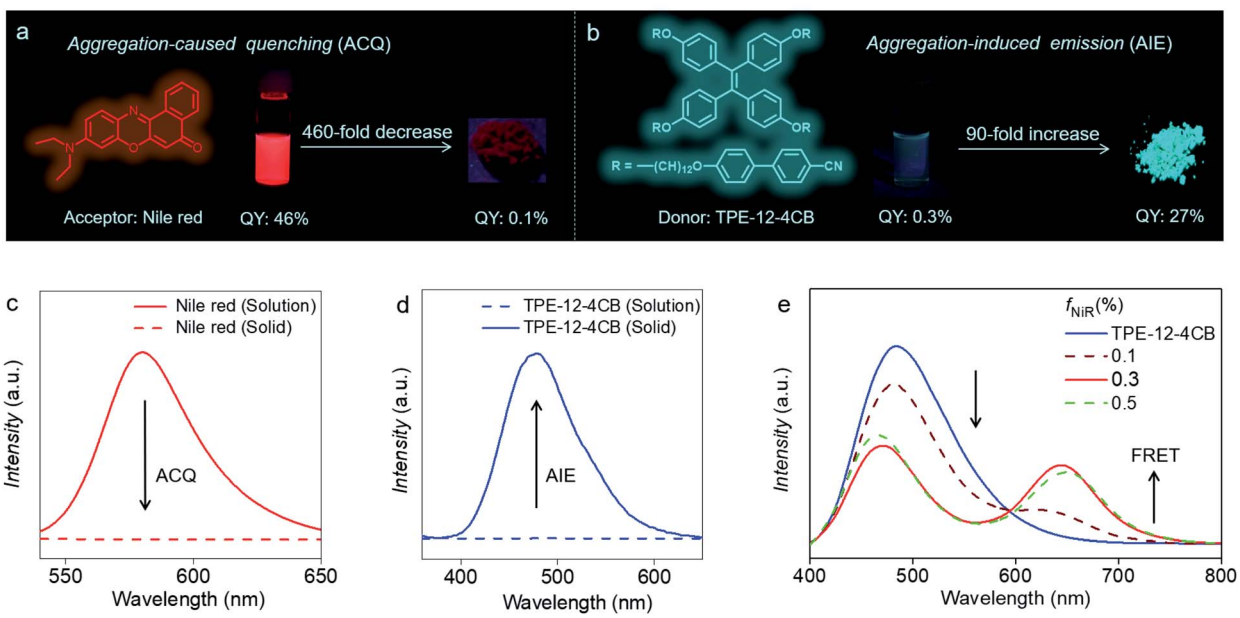

Fig. 3 Significant molecular self-assemblies and photophysical characteristics can cause either fluorescence quenching (a) or AIE-enhanced emission (b). The emission spectra of Nile red (c) and TPE-12-4CB (d) change dramatically from solution to the solid state, but in completely opposite directions. (e) Thin-film fluorescence spectra of TPE-12-4CB (donor) in the absence (solid blue) or presence of the acceptor Nile red at various molar ratios (f_{NiR}): $\lambda_{ex} = 330$ nm, 90 °C.

© 2021 The Author(s). Published by the Royal Society of Chemistry

Open Access Article. Published on 26 January 2021. Downloaded on 6/18/2025 4:34:19 AM.
This article is licensed under a Creative Commons Attribution-NonCommercial 3.0 Unported Licence.

red fluorescence from 0% fraction of Nile red (f_{NiR}) to 0.3% (molar ratio). Further increasing f_{NiR} to 0.5% causes Nile red fluorescence to diminish, indicating that co-assembly of the OIL reached its optimal ratio for FRET at 0.3% Nile red in TPE-12-4CB. This FRET maximum indicates that Nile red and TPE-12-4CB form an optimal co-assembled liquid crystal. The putative reason is that excess Nile red (>0.3%) disrupts this co-assembly of the OIL or the liquid crystallinity of the system, and consequently the FRET efficiency attenuates. These results indicate that the order of the co-assembled liquid crystal is maximized at 0.3% Nile red.

Placing the FRET pair (acceptor/donor = 0.3%) in an LC alignment cell at ~100 °C results in a LC device after cooling down to room temperature (RT). When the temperature was lower than 70 °C, FRET was switched off and blue emission of the TPE-12-4CB donor dominated. When the temperature was higher than 80 °C, Nile red co-assembled into TPE-12-4CB fully, and FRET efficiency sharply increased; thus the emission colour changed from blue to orange-red (Fig. 4b). Of particular interest is that ambient temperature can modulate the FRET efficiency.[37,38] In the process of heating to 105 °C, Fig. 4b depicts *vivid* thermochromic behaviour when the emission changes from blue to orange-red fluorescence. In particular, near the inflection point of the FRET (temperature ranges from 70 to 80 °C), an obvious fluorescence colour switching from blue to red orange was observed, indicating fast-changing of the FRET efficiency.

In order to demonstrate the temperature-controlled FRET dynamically and accurately, we set up a synchronous thermo-optical sensing (STOS) system. In this STOS system (Fig. 4a), the FRET-active LC cell was placed on a heating stage equipped with programmed temperature control, and an infrared thermal imager was used to monitor the actual temperature. Fluorescence and FRET excited at each individual wavelength are detected by the sensor tip of an optic fiber, and a CCD spectrometer was used for real-time data acquisition. Upon irradiation at 365 nm, our FRET cell responded dynamically to temperature-dependent fluorescence intensity from 30 to 105 °C (Fig. 4c). As shown in Fig. 4d, fluorescence intensity declined from the crystal state to the LC state due to the raising of temperature. The maximum emission originating from the FRET in the red-orange spectral region showed a ~40 nm blue shift because the degree of interactions between Nile red and TPE strongly altered their characteristics from the solid crystal to the liquid crystal phase, whereas the original TPE peak had no shift in the green spectral region.

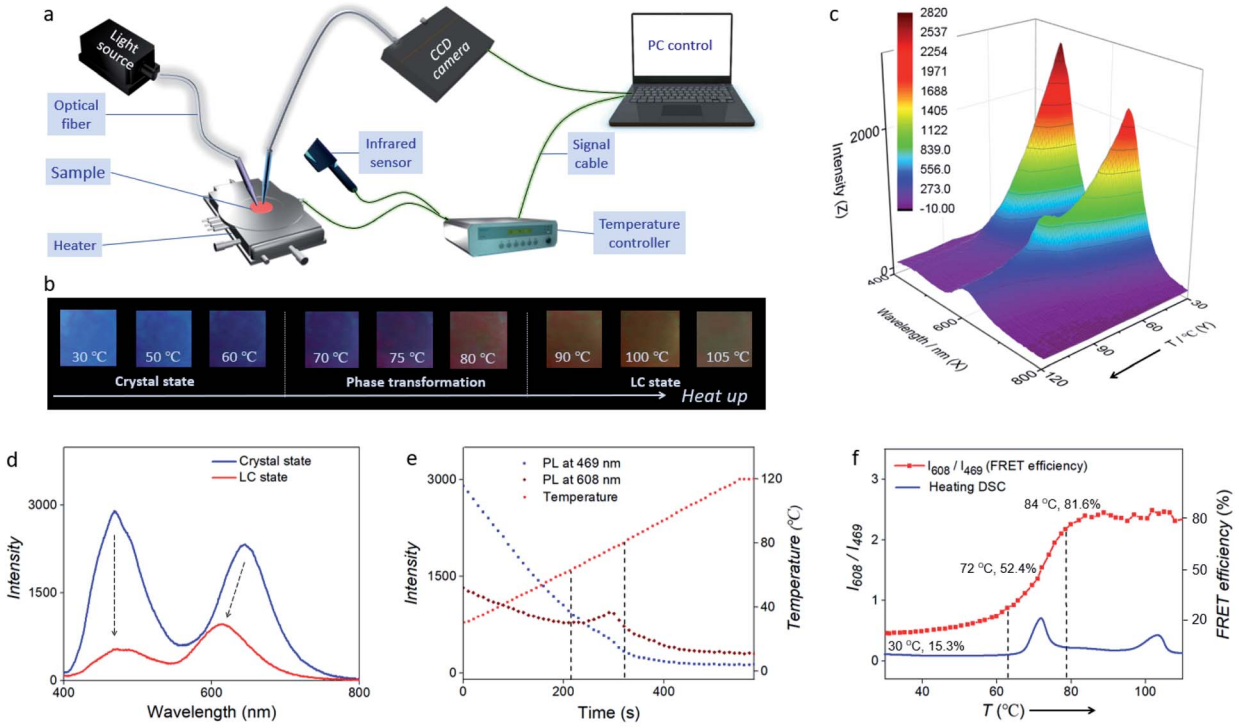

Fig. 4 (a) Setup of the original synchronous thermo-optical sensing (STOS) system *in situ* comprises a light source and a CCD camera for optical detection, a thermal infrared imager, a heating stage and its controller for the thermal control system, and a central processing computer. (b) Fluorescence photographs of a FRET-active cell demonstrating the colour change as a function of temperature, Nile red/TPE-12-4CB = 0.3% (molar ratio). (c) Three-dimensional (3D) plot, which relates fluorescence intensity (*Z*-axis) to wavelength (*X*-axis) and temperature (*Y*-axis), reveals that FRET dynamics under 365 nm excitation effectively senses the temperature variations. (d) Fluorescence intensity changes dramatically from the crystal state (blue line) to the liquid crystal state (red line) because different degrees of order control FRET and the self-assembled structures affect FRET intensity. (e) Fluorescence intensity at 469 nm originated from TPE-12-4CB (blue dot) and at 608 nm originated from Nile red (brown dot), and temperature variation was monitored synchronously by STOS. (f) Heating DSC trace of liquid crystal TPE-12-4CB, fluorescence intensity ratio (I_{608}/I_{469}) and FRET efficiency reveal that the dramatic FRET dynamics is strongly correlated with the solid-order-to-liquid-crystal-order transition at ~72 °C.

© 2021 The Author(s). Published by the Royal Society of Chemistry

Open Access Article. Published on 26 January 2021. Downloaded on 6/18/2025 4:34:19 AM. This article is licensed under a Creative Commons Attribution-NonCommercial 3.0 Unported Licence.

To further illustrate the temperature-controlled FRET mechanism, three curves collected by STOS are presented in Fig. 4e. From 0 to 580 s, the temperature of the FRET-active cell was programmatically increasing from 30 to 120 °C. Meanwhile, the fluorescence intensity at 469 nm showed an obvious recession with a tiny deviation, suggesting a rapid response of FRET to the elevated temperature. Interestingly, there was a pronounced fluctuation from 214 to 321 s in the dynamic curve of the fluorescence intensity at 608 nm. We concluded that this pronounced fluctuation was related to phase transformation into the liquid crystal. Such characteristic behaviour is different from traditional supramolecular systems, in which the FRET efficiency depends on the concentration, but here the FRET efficiency depends on the phase transition of the donor. This modulated emission (at 608 nm) maximizing during TPE-12-4CB phase transformation indicates that Nile red interacts more strongly with TPE-12-4CB in the LC state than in the solid-state crystal, supporting co-assembly formation in LCs.

Moreover, Fig. 4f depicts the temperature-dependent intensity ratio between fluorescence intensities at 608 nm from Nile red and 469 nm from TPE-12-4CB and it increases sharply from 0.9 to 2.2. Compared to and agreeing with the DSC heating curve of TPE-12-4CB, the evidence clearly shows that the FRET efficiency increased in an S-curve manner from 63 °C to 79 °C, corresponding to the phase transformation from the crystal state to the LC state. In phase transformation from the LC state to an isotropic liquid, however, almost no additional FRET change was detected from 95 to 105 °C, indicating no significant change in the structure of the Nile red and TPE-12-4CB co-assembly. Meanwhile, Fig. 4b shows that the fluorescence changed drastically during first phase transformation and weakly during second phase transformation, which corroborate the above analyses. Finally, as shown in Fig. 4e and f, the STOS signal is greatly amplified by FRET, revealing both phase transformation and non-phase transformation like general dynamic change of emissive LCs.

Conclusions

In summary, we have systematically presented a "*step-by-step*" strategy for the realization of a highly emissive liquid crystal by integrating an AIE unit into a LC, magnifying the mesogenic effect, and elongating the spacer between the AIE group and mesogens. This effectively solves the dilemma of organizing the rigid π-conjugated structure for strong emission and the flexible assembly for liquid crystallinity. Furthermore, based on the highly emissive liquid crystal, a FRET-active luminescence switching system was constructed using thermal–optical modulation. Such a system enables sensitive optical sensing of temperature and conversely accurate temperature regulates optical emission colours and dynamic switching between colours. Thus, a new thermochromic method for controlling and directing light emerges from the HELC and STOS system.

Conflicts of interest

There are no conflicts to declare.

Acknowledgements

This work was supported by the National Natural Science Foundation of China (21875143, 21674065 and 21908146), the Innovation Research Foundation of Shenzhen (JCYJ20180507182229597) and the Natural Science Foundation of Guangdong Province (2016A030312002). Special thanks to the Instrumental Analysis Center of Shenzhen University (Lihu Campus). ADQL gratefully acknowledges the financial support provided by the chemistry division of the NSF (CHE-1744362).

References

1 Y. Wu, L. H. You, Z. Q. Yu, J. H. Wang, Z. Meng, Y. Liu, X. S. Li, K. Fu, X. K. Ren and B. Z. Tang, *ACS Mater. Lett.*, 2020, **2**, 505–510.
2 (*a*) S. J. Wang, R. Y. Zhao, S. Yang, Z. Q. Yu and E. Q. Chen, *Chem. Commun.*, 2014, **50**, 8378–8381; (*b*) S. B. Chen, S. J. Jiang, J. B. Qiu, H. Y. Guo and F. F. Yang, *Chem. Commun.*, 2020, **56**, 7745–7748; (*c*) X. Yu, H. Chen, X. Shi, P. A. Albouy, J. Guo, J. Hu and M. H. Li, *Mater. Chem. Front.*, 2018, **2**, 2245–2253; (*d*) Y. Li, K. Liu, X. Li, Y. Quan and Y. Cheng, *Chem. Commun.*, 2020, **56**, 1117–1120.
3 X. Yang, J. Han, Y. Wang and P. Duan, *Chem. Sci.*, 2019, **10**, 172–178.
4 X. S. Xiao, W. Lu and C. M. Che, *Chem. Sci.*, 2014, **5**, 2482–2488.
5 L. Zhu, M. T. Trinh, L. Yin and Z. Zhang, *Chem. Sci.*, 2016, **7**, 2058–2065.
6 Y. Molard, F. Dorson, V. Cîrcu, T. Roisnel, F. Artzner and S. Cordier, *Angew. Chem., Int. Ed.*, 2010, **49**, 3351–3355.
7 W. Z. Yuan, Z. Q. Yu, P. Lu, C. Deng, J. W. Y. Lam, Z. Wang, E. Q. Chen, Y. Ma and B. Z. Tang, *J. Mater. Chem.*, 2012, **22**, 3323–3326.
8 F. Lu, K. Jang, I. Osica, K. Hagiwara, M. Yoshizawa, M. Ishii, Y. Chino, K. Ohta, K. Ludwichowska, K. J. Kurzydłowski, S. Ishihara and T. Nakanishi, *Chem. Sci.*, 2018, **9**, 6774–6778.
9 W. Zhang, T. Sakurai, M. Aotani, G. Watanabe, H. Yoshida, V. S. Padalkar, Y. Tsutsui, D. Sakamaki, M. Ozaki and S. Seki, *Adv. Opt. Mater.*, 2019, **7**, 1801349.
10 S. K. Park, S. Varghese, J. H. Kim, S. J. Yoon, O. K. Kwon, B. K. An, J. Gierschner and S. Y. Park, *J. Am. Chem. Soc.*, 2013, **135**, 4757–4764.
11 M. Martínez-Abadía, S. Varghese, B. Milián-Medina, J. Gierschner, R. Giménez and M. B. Ros, *Phys. Chem. Chem. Phys.*, 2015, **17**, 11715–11724.
12 H. W. Chen, J. H. Lee, B. Y. Lin, S. Chen and S. T. Wu, *Light: Sci. Appl.*, 2018, **7**, 17168.
13 M. Yu, R. Huang, J. Guo, Z. Zhao and B. Z. Tang, *PhotoniX*, 2020, **1**, 11.
14 P. Lin and F. Yan, *Adv. Mater.*, 2012, **24**, 34–51.
15 J. T. Mabeck and G. G. Malliaras, *Anal. Bioanal. Chem.*, 2006, **384**, 343–353.
16 X. Zhang, Y. Zhang, H. Zhang, Y. Li, Y. Quan and Y. Cheng, *Org. Lett.*, 2019, **21**, 439–443.
17 X. Yang, M. Zhou, Y. Wang and P. Duan, *Adv. Mater.*, 2020, **32**, 2000820.

© 2021 The Author(s). Published by the Royal Society of Chemistry

Open Access Article. Published on 26 January 2021. Downloaded on 6/18/2025 4:34:19 AM.
This article is licensed under a Creative Commons Attribution-NonCommercial 3.0 Unported Licence.

18 S. Yamkawa, K. Wada, M. Hidaka, T. Hanasaki and K. Akagi, *Adv. Funct. Mater.*, 2019, **29**, 1806592.
19 S. Diring, F. Camerel, B. Donnio, T. Dintzer, S. Toffanin, R. Capelli, M. Muccini and R. Ziessel, *J. Am. Chem. Soc.*, 2009, **131**, 18177–18185.
20 K. Tanabe, Y. Suzui, M. Hasegawa and T. Kato, *J. Am. Chem. Soc.*, 2012, **134**, 5652–5661.
21 V. de Halleux, J. P. Calbert, P. Brocorens, J. Cornil, J. P. Declercq, J. L. Brédas and Y. Geerts, *Adv. Funct. Mater.*, 2004, **12**, 649–659.
22 A. Schultz, S. Diele, S. Laschat, M. Nimtz and J. Hill, *Adv. Funct. Mater.*, 2002, **12**, 808–810.
23 J. Luo, Z. Xie, J. W. Y. Lam, L. Cheng, B. Z. Tang, H. Chen, C. Qiu, H. S. Kwok, X. Zhan, Y. Liu and D. Zhu, *Chem. Commun.*, 2001, 1740–1741.
24 Y. Wu, P. Jin, K. Gu, C. Shi, Z. Guo, Z. Q. Yu and W. H. Zhu, *Chem. Commun.*, 2019, **55**, 4087–4090.
25 A. C. Cavell, V. K. Krasecki, G. Li, A. Sharma, H. Sun, M. P. Thompson, C. J. Forman, S. Y. Guo, R. J. Hickman, K. A. Parrish, A. Aspuru-Guzik, L. Cronin, N. C. Gianneschi and R. H. Goldsmith, *Chem. Sci.*, 2020, **11**, 2647–2656.
26 K. Gu, W. Qiu, Z. Guo, C. Yan, S. Zhu, D. Yao, P. Shi, H. Tian and W. H. Zhu, *Chem. Sci.*, 2019, **10**, 398–405.
27 H. Li, Q. Yao, F. Xu, Y. Li, D. Kim, J. Chung, G. Baek, X. Wu, P. F. Hillman, E. Y. Lee, H. Ge, J. Fan, J. Wang, S. J. Nam, X. Peng and J. Yoon, *Angew. Chem., Int. Ed.*, 2020, **59**, 10186–10195.
28 S. L. Biesen, N. Nirmalananthan-Budau, K. Hoffmann, U. Resch-Genger and T. J. J. Müller, *Angew. Chem., Int. Ed.*, 2020, **59**, 10037–10041.
29 J. Wang, Z. Huang, X. Ma and H. Tian, *Angew. Chem., Int. Ed.*, 2020, **59**, 9928–9933.
30 O. A. Bozdemir, S. Erbas-Cakmak, O. O. Ekiz, A. Dana and E. U. Akkaya, *Angew. Chem., Int. Ed.*, 2011, **50**, 10907–10912.
31 M. R. Wasielewski, *Acc. Chem. Res.*, 2009, **42**, 1910–1921.
32 M. G. Debije and P. P. C. Verbunt, *Adv. Energy Mater.*, 2012, **2**, 12–35.
33 F. Ye, C. Wu, Y. Jin, Y. H. Chan, X. Zhang and D. Chiu, *J. Am. Chem. Soc.*, 2011, **133**, 8146–8149.
34 K. R. Raghupathi, U. Sridhar, K. Byrne, K. Raghupathi and S. Thayumanavan, *J. Am. Chem. Soc.*, 2015, **137**, 5308–5311.
35 D. Yamaguchi, Y. Ikemoto and T. Kato, *Chem. Commun.*, 2020, **56**, 9954–9957.
36 Y. Sagara and T. Kato, *Angew. Chem., Int. Ed.*, 2008, **47**, 5175–5178.
37 J. A. H. P. Sol, V. Dehm, R. Hecht, F. Würthner, A. P. H. J. Schenning and M. G. Debije, *Angew. Chem., Int. Ed.*, 2018, **57**, 1030–1033.
38 M. Chambers, M. Fox, M. Grell and J. Hill, *Adv. Funct. Mater.*, 2002, **12**, 808–810.

© 2021 The Author(s). Published by the Royal Society of Chemistry